Tellus SERIES B CHEMICAL AND PHYSICAL METEOROLOGY
PUBLISHED BY THE INTERNATIONAL METEOROLOGICAL INSTITUTE IN STOCKHOLM

Tellus (2011), 63B, 971–989
Printed in Singapore. All rights reserved

TELLUS

Observation-based 3-D view of aerosol radiative properties over Indian Continental Tropical Convergence Zone: implications to regional climate

By J. JAI DEVI[1], S. N. TRIPATHI[1]*, TARUN GUPTA[1], B. N. SINGH[1], V. GOPALAKRISHNAN[2] and SAGNIK DEY[3], *[1]Department of Civil Engineering, Indian Institute of Technology Kanpur, Kanpur 208016, India; [2]Instruments and Observational Techniques Division, Indian Institute of Tropical Meteorology, Pune 411008, India; [3]Centre for Atmospheric Sciences, Indian Institute of Technology Delhi, Hauz Khas, New Delhi 110016, India*

(Manuscript received 22 November 2010; in final form 28 July 2011)

ABSTRACT

Spatial and vertical distributions of aerosol radiative properties over Indian Continental Tropical Convergence Zone (CTCZ) up to 6 km altitude during the pre-monsoon and monsoon seasons of 2008 have been measured and reported for the first time. Inter-seasonal and intra-seasonal comparisons of different aerosol properties below and above the boundary layer are carried out in and among different regions of CTCZ. During pre-monsoon, aerosol layers were found to be present up to altitude as high as 6 km over the Indo-Gangetic Plains and Himalayan foothills. A large increase in absorption coefficients (by two to five times) near the Himalayan foothills and coastal India than the background values may be attributed to extensive biomass burning as supported by fire counts data. During monsoon, the aerosols were mostly confined to lower troposphere. However, absorbing aerosols were found to rebuild much faster than scattering aerosols after rains. Heating rates were very high over urban city of Bareilly peaking around 2 km during the pre-monsoon. The HR values over urban Kanpur during monsoon were comparable to Bareilly during pre-monsoon. Negligible latitudinal gradient of heating rate from the Himalayan foothill to central India was observed during both the seasons.

1. Introduction

Aerosols can affect the Earth's climate directly by scattering and absorbing solar and terrestrial radiation (IPCC, 2007 and references therein) and indirectly by modifying cloud properties (Twomey, 1974; Albrecht, 1989; Ackerman et al., 2000). Understanding and quantifying these effects are critical in IG Plains because several pathways have been hypothesized to explain the possible impacts of aerosols on the regional hydrological cycle that influences the livelihood of nearly one-sixth of the world's population. However, the aerosol-hydroclimate link remains unresolved and debated (Ramanathan et al., 2001, 2005; Lau et al., 2006). For example, advancement in early monsoon precipitation has been proposed by Lau et al. (2006) due to an elevated heat pump (EHP) effect from accumulation of absorbing aerosols over the Indo-Gangetic (IG) plain and Tibetan plateau during the pre-monsoon (Mar–May) season. On the contrary, Ramanathan et al. (2005), using an ensemble of coupled ocean atmosphere simulations from 1930 to 2000, proposed a weakening of the Indian monsoon circulation because of the reduction in sea surface temperature gradient due to large surface cooling induced by aerosols.

A 3-D distribution of aerosol optical and microphysical properties is required to address this issue. Satellites provide columnar aerosol properties in a high space–time frequency (Remer et al., 2008; Kahn et al., 2009), but those retrievals are very sensitive to the vertical distribution of aerosols that strongly influences the aerosol radiative forcing estimates (Ganguly et al., 2005; Chand et al., 2009). Moreover, quantifying aerosol absorption is a challenge to the satellite retrievals (Zhu et al., 2011). Total Ozone Monitoring Spectrometer (TOMS) absorbing aerosol index (AAI) has been used to quantify the absorbing aerosols, but its sensitivity to aerosols above the boundary layer (Mahowald and Dufresne, 2004) limits its use only to the pre-monsoon season. Launch of CALIOP (Cloud-Aerosol Lidar with Orthogonal Polarization) onboard CALIPSO (Winker et al., 2004) provides an opportunity to continuously monitor aerosol vertical distribution, but it also requires vertical in situ observations for retrieval

*Corresponding author.
E-mail: snt@iitk.ac.in
DOI: 10.1111/j.1600-0889.2011.00580.x

assessments. Realizing the need of in situ observations for improved aerosol characterization in this region, two major campaigns were carried out in India in recent years. Simultaneous measurements of aerosol physical, chemical and optical properties during Indian Space Research Organization-Geosphere Biosphere Program (ISRO-GBP) land campaign (Moorthy et al., 2005; Tripathi et al., 2006; Nair et al., 2007) have reduced the uncertainty in regional aerosol direct radiative forcing (Ganguly et al., 2005; Pant et al., 2006; Dey and Tripathi, 2007, 2008). The measurement of aerosol vertical distribution up to 1.5 km in the Continental Tropical Convergence Zone (CTCZ) was carried out over Kanpur during this campaign in the winter of the year 2004 (Tripathi et al., 2005, 2007). Vertical measurements up to 1.5 km provided useful information during winter because aerosols were confined to the boundary layer, but during summer season aerosols get convected up to higher altitudes. The Integrated Campaign of Aerosols, gases and Radiation Budget (ICARB) campaign during the pre-monsoon season of the year 2006 was initiated to address this issue, but it only covered the eastern part of the CTCZ (Bhubaneswar) (Babu et al., 2008; Murugavel et al., 2008) while focusing mostly on the peninsular India and surrounding oceans. Babu et al. (2008) found a nearly steady BC concentration (M_{BC}) of 1.4 $\mu g\ m^{-3}$ up to 3 km altitude and a remarkable increase in BC mass fraction (F_{BC}) with altitude over Bhubaneswar (see location in Fig. 1), while Satheesh et al. (2009) have found elevated aerosol layers between 2 and 4 km altitude above the atmospheric boundary layer. The previous two campaigns focused on the aerosol characteristics during the winter (December–February) and pre-monsoon (March–May) seasons, respectively.

CTCZ campaign, results of which are presented here, focused on the aerosol distribution in the pre-monsoon and monsoon (June–September) seasons of the year 2008, covering the continental part of the more common tropical convergence zone over India. CTCZ is characterized by intense convergence and cyclonic vorticity within and above the boundary layer respectively, and organized deep moist convection sometimes referred to as the monsoon trough (CTCZ science plan, 2008). Wang et al. (2009) using an interactive aerosol-climate model showed that the presence of absorbing aerosols can perturb the moist static energy in sub-cloud layer leading to more rainfall in the pre-monsoon months of April and May and reduction in the rainfall during monsoon months of June, July and August over CTCZ region. Therefore, this region is of great importance to study the effect of aerosols on monsoon precipitation and therefore on regional climate. Existing measurements in the CTCZ (Fig. 1) have suggested both natural (mineral dust and marine) and anthropogenic sources (industries, vehicular exhaust, biomass/biofuel burning) of aerosols in these seasons (Dey et al., 2004; Chinnam et al., 2006; Dey and Di Girolamo, 2010). Columnar measurements of spectral aerosol optical depth (AOD) along with microphysical and other optical properties near the surface at the ISRO-GBP network sites fail to represent the columnar characteristics due to presence of aerosol layers aloft. For example, surface aerosol mass concentration does not increase with increase in AOD proportionately over locations as observed over Vishakhapatnam and Maldives (Niranjan et al., 2007; Corrigan et al., 2008). Lack of adequate in situ measurements over the CTCZ region despite large space–time heterogeneity in the aerosol properties during the pre-monsoon and monsoon seasons as observed by satellite (Dey and Di Girolamo, 2010) because of mixing of natural dust aerosols transported from the Great Indian Desert in Rajasthan and the Arabian peninsula (Singh et al., 2004; Mishra and Tripathi, 2008; Mishra et al.,

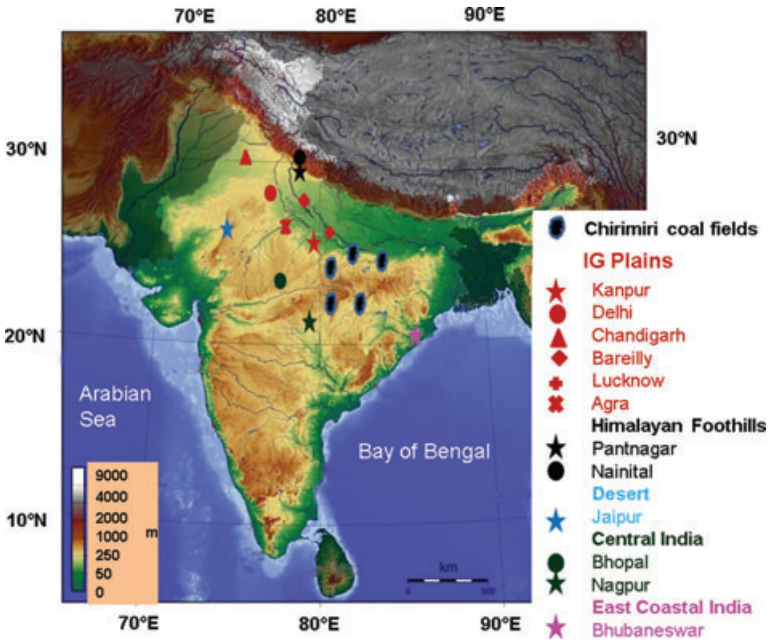

Fig. 1. Indian Continental Tropical Convergence zone (I-CTCZ) over India. Different regions are denoted by different symbols. Chirimiri coal fields are also shown in a different symbol. The regions are divided based on the dominant sources/types of aerosols present.

2009) and the anthropogenic aerosols emitted locally from the IG plain, transportation of aerosols along the slope of the Himalayan mountain range and the influence of active and break phases of the monsoon, emphasizes the need for more observations particularly of the aerosol vertical distribution. Such heterogeneity in aerosol distribution and a large uncertainty in emission factors of various anthropogenic and natural sources hinder climate models in reproducing the AOD distribution measured by satellites (Ganguly et al., 2009). Even, satellites have retrieval biases due to the complex aerosol characteristics in this region (Kahn et al., 2009; Dey and Di Girolamo, 2010). The in situ observations of aerosol microphysical properties can be valuable resources to evaluate satellite data, but they are only available from five Aerosol Robotic Network (AERONET) sites within Indian CTCZ.

The major objective of the CTCZ campaign under Indian Climate Research Program was to fill the gap in observational data by measuring the spatial and vertical gradients of various aerosol and cloud parameters within the CTCZ region (Fig. 1), using an airborne platform during the months of May and September (representative months of the pre-monsoon and monsoon seasons, respectively) in the year 2008. Here, we report the 3-D distributions of aerosol scattering, absorption and mass properties and their impacts on direct radiative forcing over the Indian CTCZ for the first time. The measurement sites are described in Section 2, followed by instrumentation and data analysis in Section 3, discussion of the results in Section 4, estimations of aerosol direct radiative forcing in Section 5 and major conclusions in Section 6.

2. Regional characteristics

The CTCZ over India has a complex topography, which varies from sea level up to 6 km. The region is composed of the Great Indian Desert in the northwest; heavily polluted IG Plains in the north-central region, Himalaya mountain range in the north and peninsular region towards south. In this study, results are discussed keeping in mind the different topographic, emission and meteorological characteristics in these five regions: (i) desert, (ii) IG Plains, (iii) Himalayan foothills, (iv) central India and (v) coastal India.

2.1. IG plain

The IG Plain stretches from Pakistan in the west to Bangladesh in the east encompassing a large fraction of northern and eastern India (Abrol et al., 2002), but this study is confined only to the Indian part of the IG plain. This region is the major source of anthropogenic aerosols throughout the year, whereas natural dust shows seasonal peak during the pre-monsoon and monsoon seasons (Tripathi et al., 2005; Dey and Tripathi, 2008), thus allows a possible mixing between anthropogenic and natural particles (Chinnam et al., 2006; Dey et al., 2008).

2.2. The Great Indian Desert

The Great Indian Desert covering an area of 320,000 km^2 is hot and arid with intense Aeolian activity. A detailed description of the Great Indian Desert is given in Yadav and Rajamani (2004). The high intensity S–SW surface winds at a maximum strength of 25–30 $km\,h^{-1}$ during pre-monsoon months raise a tremendous amount of dust from the loose sandy soil of the region in the order of 30–60 $kg\,m^{-2}\,day^{-1}$ (Sikka, 1997), which is transported eastward. This is the major source of dust aerosols from the pre-monsoon season through monsoon (Dey et al., 2004; Chinnam et al., 2006). Anthropogenic sources such as clay mines and gypsum quarries add to the aerosol source inventory in addition to the natural dust.

2.3. Himalayan foothills

The role of mountains in the Asian monsoon circulation was investigated in a simulation study by Hahn and Manabe (1975). Lau et al. (2006) incorporated the aerosol direct radiative effects and showed that the aerosols accumulated over the slopes of Tibetan plateau and Himalayas (Gautam et al., 2009a) during the pre-monsoon season may potentially alter the monsoon circulation. Accumulation of dust, transported from arid regions in the west, was observed over Manora peak (29°22′N, 79°27′E, 2000 m AMSL) in central Himalayas during pre-monsoon (Sagar et al., 2004). Satellite-based aerosol climatology reveals very different particle microphysical properties along the Himalayan foothills in the pre-monsoon and monsoon seasons relative to the IG Plains and Tibetan Plateau (Dey and Di Girolamo, 2010), which was hypothesized to be the effect of mountain valley breeze transport under the influence of strong boundary layer diurnal cycle (Dumka et al., 2008).

2.4. Coastal India

The peninsular India on the east bordering Bay of Bengal was covered during the study. Fourty-eight hour NOAA Hysplit back trajectory (Draxler and Hess, 1998; Draxler and Rolph, 2011) analysis at 2 km (Figs 2a and b) for pre-monsoon and monsoon season showed that the air masses to the coastal areas are dominantly from northwest and west respectively. Although the continental aerosols dominate during pre-monsoon, marine aerosols from the Arabian Sea, Bay of Bengal and continental aerosols from central India contribute to the aerosol loading over the region during the monsoon. Elevated layers of BC at 0.8 and 2 km were observed during ICARB campaign in March 2006 over the region (Babu et al., 2008). From the micro-pulse lidar (MPL) measurements of vertical profile of aerosol backscatter at Visakhapatnam (17.7°N, 83.3°E) (near to the present profiling region), Niranjan et al. (2007) found that aerosol layers with increased extinction and having a few kilometre thickness at the height between 1.6 and 5 km existed during the summer months

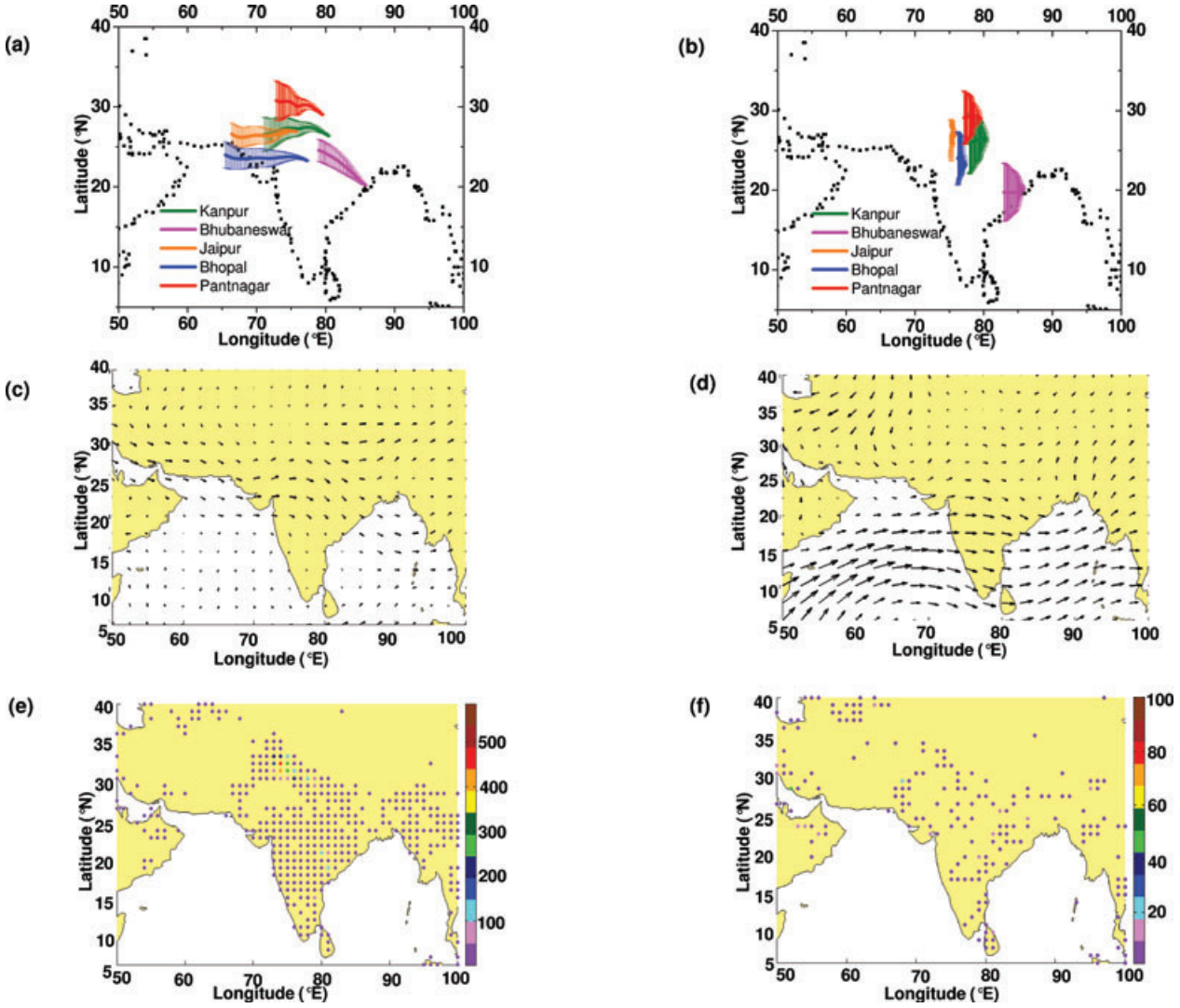

Fig. 2. Hysplit backtrajectories to Kanpur (IG Plains), Pantnagar (Himalayan foothills), Jaipur (desert), Bhubaneswar (coastal) and Bhopal (central India) at 2 km for (a) May (pre-monsoon) and (b) September (monsoon) 2008. Different colours represent backtrajectories to different regions as shown in legend. (c,d) The wind vector plot over CTCZ regions during pre-monsoon (MAM) and monsoon (JJAS) of 2008, respectively. Northwesterly winds can be clearly seen during the pre-monsoon. Solid circles showing the MODIS fire counts for (e) pre-monsoon (May 2008) season and (f) monsoon season (September 2008) while different colours show the number of fire counts which can be interpreted from the colour bars.

(March–April) of 2005 and 2006. Das et al. (2009) showed an increase in the AOD with a corresponding decrease in wavelength exponent (α) to zero and negative values indicating the dominance of coarse mode particles during the early monsoon months.

2.5. Central India

Central India is bordered with the Great Indian Desert in the northwest, IG plain in the north and coastal India in east, west and south. Ganguly et al. (2005), through ground-based measurements from Hyderabad to Ahmadabad in February 2004, found high spatial variability due to unequal changes in source strength or removal processes of aerosols. Presence of elevated layers was found in central India (Bangalore) during the pre-monsoon season by Satheesh et al. (2008).

2.6. Synoptic meteorology

The 48 hours NOAA HYSPLIT back-trajectory plots at 2 km AMSL show strong westerly and northwesterly air mass during pre-monsoon (May 2008; Fig. 2a) while the air mass

arrives from all directions during monsoon (September 2008; Fig. 2b) over CTCZ. The synoptic wind patterns at 850 mbar over the Indian subcontinent during pre-monsoon and monsoon are shown in Figs 2c and d (Kalnay et al., 1996). Strong westerly to northwesterly winds are prominent during pre-monsoon and wind comes from all directions during monsoon similar to the back trajectories. Figure 2e shows the fire spots (Davies et al., 2009) predominantly due to biomass burning (forest fires and crop residue burning) (Venkataraman et al., 2006; Vadrevu et al., 2008; Beegum et al., 2009) in May 2008 which is apparently high as compared to September 2008 (Fig. 2f). Therefore, during the pre-monsoon season in CTCZ, the wind carries desert dust from the Middle-East and the Great Indian Desert, biomass burning aerosols from the northwest and the anthropogenic aerosols from the IG Plains (Sagar et al., 2004; Lau et al., 2006). These aerosols get piled up over the foothills and convected to higher altitudes due to very high temperature over the land surface (Prospero et al., 2002; Gautam et al., 2009a).

Pre-monsoon season is characterized by high temperatures (28.5 to 41.3 °C) over CTCZ (http://www.imd.gov.in/doc/climateimp.pdf) except the Himalayan foothills where it is between 16.3 and 23.5 °C, and dry (relative humidity, RH $\leq$ 50%) heat wave condition over north and central India. Monsoon is characterized by seasonal rainfall all over India. The surface temperature gradually decreases with the onset of monsoon rains over the regions and the RH soars to ∼80%. The monsoon rains show high regional variability (http://www.imd.gov.in/section/hydro/srnormals/Monsoon.gif) with a normal (30 years average) of 262.8 mm over desert, 1223.1 mm over Himalayan Foothills, 1164.9 mm near the east coast of India and 993.9 mm over central India.

3. Measurements, instrumentation and analysis

Measurements were carried out both within (∼1 km) and above (∼3 km) the boundary layer from IG Plains to different zones during May 27–31 in the pre-monsoon and 03–15 September in the monsoon seasons. Vertical profiling up to 3 km was carried out over Kanpur, Delhi, Chandigarh and Bareilly in IG Plains, Pantnagar in Himalayan foothills, Jaipur near the Great Indian Desert, Indore in central India and Bhubaneswar in coastal India. The details of scientific flight paths are given in Table 1.

A pressurized twin turbo prop executive aircraft Super King Air B 200 from the National Remote Sensing Centre (NRSC), Hyderabad, India, was used for the study. The list of instruments deployed in the aircraft for measuring the aerosol microphysical and optical properties and their sampling frequencies are summarized in Table 2. The sampling inlets of the instruments were protruded out from the belly of the aircraft. Scanning Mobility Particle Sizer (SMPS), Aerodynamic Particle Sizer (APS) and aethalometer were connected to a community inlet whereas Photoacoustic Soot Spectrometer (PASS) had separate sampling inlet. The inlets were mounted forward facing and were 10 cm lower and 5 cm farther from the exhausts located at the back of inlets so that the inlet air is not contaminated with the exhaust air from instruments. Maneuvering at different levels at a minimum interval of 300 m vertically and bigger diameter (>5 km) during multilevel profiling avoided the contamination of aircraft / instrument exhaust into the inlet. The working principle and error

Table 1. *Details of scientific flights during the experiment*

Date	Sortie	Time of flight (h IST)	Height of flight (km AMSL)
Pre-monsoon			
May 29	Bhopal–Aurangabad	08:43–10:03	3
	Aurangabad–Nagpur	11:23–12:32	3
	Nagpur–Bhubaneswar	13:10–14:44	3
	Bhubaneswar–Kanpur	15:36–18:07	3
May 30	Kanpur–Pantnagar–Bareilly–Kanpur	11:02–13:11	3–3-1
May 31	Kanpur (Multilevel)	12:35–14:29	3–2
Monsoon			
September 4	Kanpur (Multilevel in FN and AN)	08:58–10:29	Spiraling at different levels from 4.5 to 0.5 km
		11:57–13:21	
September 5	Kanpur–Delhi–Kanpur	09:24–11:57	1.2–2.1 km with 2.7 km over Aligarh
September 9	Kanpur–Pantnagar–Bareilly–Nainital–Kanpur	10:26–13:00	1.2–3-2–3
Sep. 10	Kanpur–Chandigarh–Kanpur	09:13–11:10	3–6 (due to Cb clouds)
September 11	Kanpur–Jaipur	09:05–11:53	Stair flights
September 12	Kanpur–Bhubaneswar	09:28–12:24	1.6
September 14	Kanpur–Indore–Nagpur–Bhubaneswar	09:29–16:23	3–2.3–2.7
September 15	Bhubaneswar—Nagpur–Indore–Kanpur	09:30–16:41	4–4-4

IST, Indian standard time; AMSL, above mean sea level.

Table 2. *List of instruments used in the aircraft along with their specifications*

Instrument/make/model	Parameter(s) measured	Temporal resolution (or sampling frequency)	Season
Optical properties			
Photoacoustic soot Spectrometer/Droplet Measurement Technologies/PASS1	Absorption and scattering coefficient (wavelength = 870 nm)	1 s	Pre-monsoon and monsoon
Microphysical properties			
Scanning mobility particle sizer/TSI, Inc./3696	Particle size distribution (3–1000 nm)	1.5 min	Monsoon
Aethalometer/Magee Scientific/AE-21-ER	BC mass concentration at two wavelengths (370 and 470 nm)	3 min	Monsoon
Aerodynamic particle sizer/TSI, Inc./3321	Particle size distribution (0.3–20 μm)	20 s	Monsoon

budget of the instruments are given in the following sections. A DMT Cloud Condensation Nuclei Counter (CCNC) has been used for measuring cloud condensation nuclei. The working principle of CCNC is explained in detail in Good et al. (2010). The details about spectro-radiometer which was also installed in the aircraft are given elsewhere (Jethva et al., 2009).

3.1. Instrument description

3.1.1. Photo acoustic soot spectrometer (PASS). The PASS, integrated with a photomultiplier tube, measures absorption coefficient (b_{abs}) and scattering coefficient (b_{scat}) every second at 870 nm wavelength. Measured b_{abs} is proportional to the acoustic signal from the pressure wave generated from the local rise in temperature as a result of absorption of modulated laser power by aerosols. A detailed description can be found in Arnott et al. (1999). b_{scat} were measured simultaneously by use of the photomultiplier tube configured in PASS to operate as a reciprocal nephelometer by measuring the scattered optical power using a cosine weighted detector. The details are given in Lewis et al. (2008). The diffusion losses in the size range from 10 nm to 1 μm were within 10% for both the measurements. b_{scat} was corrected for background scattering which is the amount of light scattered by the windows, mirror, wall etc. and by Rayleigh scattering (Lewis et al., 2008). The instrument was factory calibrated before the experiment. The b_{abs} measurements have a 5% relative uncertainty, whereas the b_{scat} measurements have a systematic relative uncertainty of 15% (Lewis et al., 2008).

The instrument was housed inside the aircraft cabin where the sample was drawn at 1 LPM through conductive tubing from the inlet to minimize losses in sampling lines by reducing the buildup of static charge (Fig. 3a). An acoustic resister, a 6-cm-long brass tube, was placed near the instrument inlet to dampen the ambient pressure fluctuations at lower altitudes (Arnott et al., 2006) thereby reducing the noise due to turbulence. Occasionally higher temperatures up to 42°C in the aircraft cabin during the pre-monsoon season caused laser power to fluctuate. In the subsequent analysis, b_{abs} and b_{scat} data with high laser power fluctuations more than 2 mW (between two consecutive points) were excluded. Running averages of 300 points were done on b_{abs} to further reduce the noise in measurement to 10 Mm^{-1}. To get a better comparison, 301 point running average was done for b_{scat} as well in all the data sets.

The RH plays a vital role in both b_{abs} and b_{scat} measurements due to the hygroscopic growth of most atmospheric aerosols. Using a reciprocal nephelometer operating at 870 nm, Lewis et al. (2009) showed increase in b_{scat} values beyond 74% RH for biomass smoke aerosols, whereas Fierz-Schmidauser et al. (2009) using an integrating nephelometer showed an increase in b_{scat} values by a factor of 1.1–1.8 at 80% RH compared to dry aerosols. b_{abs} systematically decreases beyond 70% RH due to contribution of mass transfer to the photoacoustic signal (Arnott et al., 2003). They found that at 80% RH, b_{abs} decreases by 8%. The RH during the pre-monsoon season was less than 40%, indicating dry aerosols whereas during the monsoon season, RH increased to 80% at lower altitudes.

3.1.2. Aethalometer. Aethalometer (model AE-21-ER; Magee Scientific, Berkeley, CA, USA) was installed inside the aircraft cabin with the sampling inlet connected to the belly of the aircraft (Fig. 3a). Because the aircraft operated in pressurized mode, a diaphragm pump was used to aid the instrument in drawing air from the inlet without any size selective inlet. The instrument was operated at a flow rate of 5 LPM and sampling frequency of 3 min, and the data for flow rate <4.7 LPM due to pressure fluctuations were discarded. Losses due to the presence of pump were found to be within 3%, which is within the acceptable limit for analysis. No pressure correction was required even during ascend and descend of the aircraft as the setup made

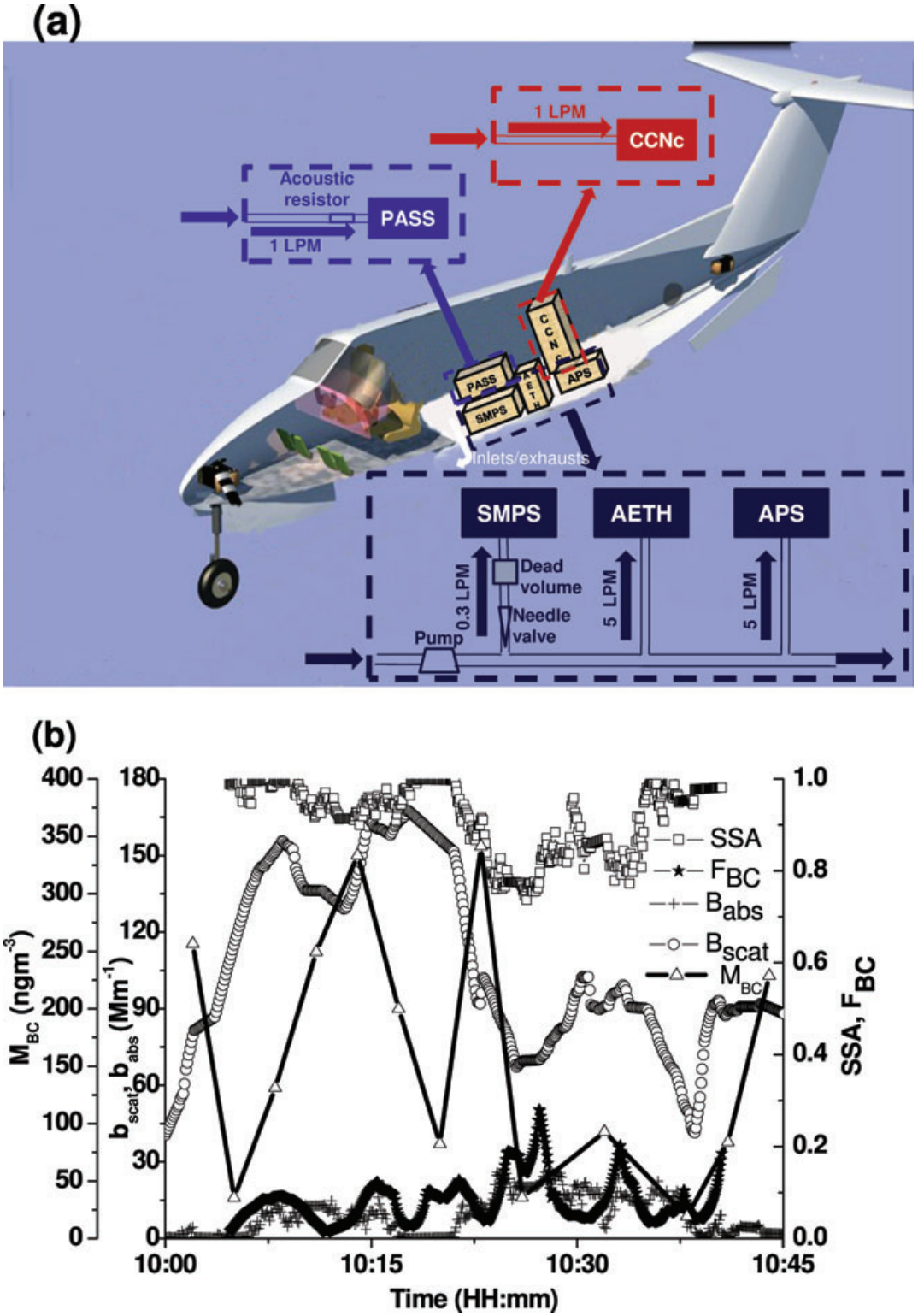

Fig. 3. (a) The setup of PASS inside the aircraft cabin. A small copper tube (as acoustic resister) near the PASS inlet was used to dampen the ambient pressure fluctuations. Setup of SMPS, aethalometer and APS inside the aircraft cabin is also shown. An orifice and dead volume was used to control the flow rate in SMPS as shown. CCNC inlet was directly connected to the main inlet. (b) Shows 45 min time-series analysis for a leg from Kanpur to Pantnagar, 9 September. Figure shows optical (b_{abs}, b_{scat}, SSA) properties obtained from PASS in the primary Y-axis and BC fraction obtained from aethalometer and total mass from SMPS and APS is shown in the secondary Y-axis. X-axis shows local standard time (IST).

for measurements inside the aircraft provided surface pressure conditions. The instrument has an overall uncertainty of 10% (with a minimum of 100 ng m^{-3}) for M_{BC} (Babu and Moorthy, 2002; Tripathi et al., 2005).

3.1.3. Scanning mobility particle sizer (SMPS). SMPS (Model 3936; TSI Inc. Shoreview, MN) measures the aerosol size distribution from 16.8 nm to 572 nm with a time base of 90 s (up scan: 60 s) and a set sample flow rate of 0.3 LPM and sheath flow rate of 3 LPM. The particles in this size range are classified based on their mobility diameter using an Electrostatic Classifier (Model 3080; TSI Inc.) with a differential mobility analyser (Model 3081; TSI Inc.) and counted using a Condensation Particle Counter (Model 3775; TSI Inc.). For the instrument to work in pressurized mode at high altitudes, an auxiliary pump, an orifice and a dead volume were used to aid in maintaining a constant flow rate even at higher altitudes and during ascend and descend (Fig. 3a). Leak tests on the instruments were performed on ground and in-flight periodically.

The number concentration (N_F) of the instrument was converted to mass concentration (M_F), assuming the particles to be spherical with a density of 1.67 g cm^{-3}. This density is in the range (1.54–1.77 g cm^{-3}) given by McMurry et al. (2002) for urban atmospheric aerosols of ∼0.1 and ∼0.3 μm mobility diameter. Because the flow rate of SMPS was very low, diffusional losses due to the length of the pipe may be of concern. The transport efficiency for a 20 nm particle (Baron and Willeke, 2001) was found to be 88%. Thus, it can be safely assumed that the transport efficiency for bigger particles will be much higher. Impaction and interception losses, even though very little for such tiny particles, also occurred due to the position of pump and orifice before the instrument inlet in the aircraft during flow control. The particle losses were duly accounted by estimating the losses under artificial vacuum conditions created in the laboratory. A chamber with low pressure (up to 600 mbars) was maintained and the instrument sampling inlet was kept inside it. The losses in sampling were estimated by comparing the number concentrations at atmospheric versus low-pressure conditions for each particle size bin.

3.1.4. Aerodynamic particle sizer (APS). APS (3321; TSI Inc.) measures the aerosol size distribution from 0.542 to 20 μm aerodynamic diameter, using the time of flight particle sizing technology in which the acceleration of aerosol particles are measured in response to the accelerated flow of the sample aerosols through a nozzle. The frequency of measurement was set as 20 s. The sampling was carried out through teflon tubing from the inlet. The flow rate of the instrument was set as 5 LPM with a sample flow rate of 1 LPM and a sheath flow of 4 LPM. The number distribution obtained from APS was later converted to mass concentration using a density of 1 g cm^{-3} as the measurement carried out was aerodynamic diameter. The accuracy in the measurement is ±10% of the reading plus variation from counting statistics (Model 3320, APS instruction manual). No correction for pressure was applied to the measured data as the instrument automatically corrects the data between 400 and 1030 mbar, which cover the measurement pressure range.

3.2. Analysis

SMPS and APS distributions were merged to obtain the number distribution of the aerosols in the size range from 0.0168 to 20 μm. Mobility diameter from SMPS, which was converted to aerodynamic diameter using the following equation with the help of DataMerge software module (Model 390069; TSI Inc.):

$$d_a = d_m \left[\frac{C(d_m)}{C(d_a)}\right]^{\frac{1}{2}} \left(\frac{\rho_p}{\chi \rho_o}\right)^{\frac{1}{2}}, \quad (1)$$

where ρ_p is the particle density, ρ_o the reference density 1 g cm^{-3} and χ is the dynamic shape factor. m and a denote mobility and aerodynamic diameters, respectively. $C(d)$ is the slip correction:

$$C_c = 1 + \frac{2\lambda}{D_p}\left(1.142 + 0.558e^{\frac{-0.999C_p}{2\lambda}}\right), \quad (2)$$

where λ = mean free path = 66.5 nm and D_p is the particle diameter.

Because APS gives the size distribution every 20 s and SMPS in 90 s, APS data were averaged to merge with the SMPS data for the same time period to merge the size distribution for different time periods.

3.3. Heating rate (HR) calculations

Vertical and spatial measurements of b_{scat}, b_{abs}, *SSA*, total mass concentration (M_T) and M_{BC} were carried out covering all the regions of CTCZ. M_T and M_{BC} were measured only during the monsoon experiment. Vertical measurements over key stations such as Kanpur, Pantnagar and Bhubaneswar, etc. covered up to 3 km altitude during pre-monsoon and monsoon except over Kanpur where it was up to 6 km during monsoon. For the locations with vertical measurements, aerosol direct radiative forcing (DRF) in the short wave (0.25–4 μm) was estimated using SBDART (Santa Barbara DISORT Atmospheric Radiative Transfer; Ricchiazzi et al., 1998), a plane-parallel radiative transfer model, and then HR was calculated. For the calculation of DRF and consequently HR, optical properties such as b_{ext}, *SSA* and asymmetry parameter (g) were required spectrally in the shortwave region. b_{ext} and *SSA* were measured at 870 nm only due to instrument constraints. A user-defined model was, therefore, developed using optical properties of aerosol and clouds (OPAC; Hess et al., 1998) for each location at all measured altitudes by varying the number density of different aerosol components which are dominant in the location to retrieve the aerosol properties required as input to SBDART. The user-defined models at each altitude for different locations were constrained such that the following conditions are satisfied: (i) The modelled and observed parameters agree within ±5% tolerance for optical properties (b_{ext} and *SSA* at 870 nm) and ±10% for mass

properties. (ii) The quantity, σ, obtained from the columnar AOD from OPAC and the columnar AOD spectrally at ≥4 wavelengths from AERONET/MODIS is less than 0.04 considering the retrieval error of observed AOD. σ is defined as

$$\sigma = \sqrt{\frac{1}{N}\sum_{\lambda=1}^{n}\left(\mathrm{AOD}_{\lambda,\mathrm{AERONET/MODIS}} - \mathrm{AOD}_{\lambda,\mathrm{MODEL}}\right)^2}. \quad (3)$$

When the above conditions were satisfied, the optical properties such as b_{ext}, *SSA* and g were retrieved spectrally at RH close to ambient RH.

The columnar AOD from AERONET/MODIS were used to calculate the AOD above the measured top altitude (hereafter, referred as top altitude). This AOD above the top altitude was again constrained using OPAC by optimizing the transported mineral dust density at altitudes seen from CALIPSO images and extrapolating the number density of aerosols at top altitudes ∼3 to 20 km. The AOD was retrieved at all wavelengths from 0.25 to 4 μm. The columnar AOD from OPAC was, then, a sum of extinction optical depth up to the top altitude and above that.

During monsoon, the hygroscopic property affect the optical properties and hence, the radiative forcing to a great extent. To account for this effect, the aerosol properties were retrieved from OPAC at realistic RH at each altitude. In addition to the optical properties, other inputs such as columnar ozone, columnar water vapour and surface albedo are required as inputs to SBDART. Standard atmospheric profiles of temperature and pressure for tropical atmosphere were used to perform radiative forcing calculations. Columnar ozone data were obtained from Total Ozone Mapping Spectrometer (TOMS) and water vapour data were obtained from Atmospheric Infrared Sounder (AIRS). Surface reflectance data were taken from MODIS at seven wavelength bands centred at 0.470, 0.555, 0.648, 0.858, 1.24, 1.64 and 2.13 μm. Optical properties such as SSA, AOD, g along with other surface properties, atmospheric properties, etc. were incorporated in SBDART to obtain DRF. SBDART utilized these data to calculate net RF for a user-defined spectral range (0.25 to 4.0 μm) at different solar zenith angles (SZA) (with a resolution of 10°) at different altitude levels. The diurnal averaged forcing ($\Delta F_{\mathrm{TOA/S}}$) are calculated by

$$\Delta F = \frac{1}{2}\int_0^1 \Delta F(\mu_0)\,\mathrm{d}\mu_0, \quad (4)$$

where μ_0 is the cosine of SZA (Dey and Tripathi, 2007).

SBDART provides values of TOA forcing (with and without aerosol) along with surface forcing (with and without aerosol) and flux in and flux out at each altitude level. These values have been used to calculate net RF for the particular layer at different SZA. The forcing values at different SZA are averaged to calculate total diurnal forcing subsequently used to calculate HR as followed in Tripathi et al. (2007).

4. Results and discussions

The results of the CTCZ campaign are reported separately for the pre-monsoon and monsoon seasons. Measurements were carried out from IG Plains (Kanpur) to Himalayan foothills and coastal India during the pre-monsoon and from IG Plains (Kanpur) to Desert, Himalayan foothills, central and coastal India during the monsoon seasons. Figure 3b shows a time-series plot of different parameters during an aircraft sortie from Kanpur to Pantnagar. Overall, the real-time data from different instruments look self-consistent. For instance, the region with high F_{BC} corresponds to low SSA, whereas M_{BC} peaks coincide with b_{abs} except at 10:12 because of the difference in frequency of measurement, that is 3 min for M_{BC} against 1 s for b_{abs}.

4.1. Aerosol characteristics during pre-monsoon

4.1.1. IG Plains and Himalayan foothills. Multilevel profiles of b_{ext} and SSA at 0.91, 2.1, 2.9 and 3.3 km on May 31 over rural area about 200 km east of Kanpur city centre are shown in Figs 4a and b. The 3-D variations of the same properties over the Himalayan foothills and IG Plains above (3 km) and below (1 km) the boundary layer on May 30 are shown in Figs 4c and d.

b_{ext} over Kanpur between 0 and 3.3 km altitudes was in the range 65–120 Mm^{-1} with a mean (±SD, σ) of 100 ± 4 Mm^{-1} on May 30, whereas it varied between 4 and 129 Mm^{-1} with a mean (±σ) of 27 ± 30 Mm^{-1} on the next day. These lower values indicate cleaner conditions below 3.3 km in the rural areas around Kanpur, whereas SSA below 3.3 km showed the dominance of absorbing aerosols. Aerosol layers above 4 km, possibly transported dust, were seen from CALIPSO on the day of sampling (Appendix S1). The observed columnar AOD ($\mathrm{AOD}_{\mathrm{obs}}$) at 870 nm wavelength up to 3.3 km was 0.11, whereas AERONET retrieved AOD ($\mathrm{AOD}_{\mathrm{AER}}$) at the same time in the study site at a mobile AERONET station (Mobile_N_053108E) setup for the NASA's TIGERZ campaign (http://tigerz.gsfc.nasa.gov/reports.html) was 0.22 suggesting 50% contribution to columnar AOD came from aerosols above 4 km; 37% and 15% contributions to $\mathrm{AOD}_{\mathrm{AER}}$ over Pantnagar and Bareilly respectively, came from aerosols above 3 km. The presence of aerosols layers, possibly dust, up to 6 km is evident from CALIPSO on the night of May 30 (Appendix S1).

4.1.2. Coastal India to IG Plains. The b_{ext} (±1σ) over Bhubaneswar (51 ± 4 Mm^{-1}) was comparable to Kanpur on May 31, whereas the b_{abs} (4.6 ± 0.6 Mm^{-1}) was 33% lower than that in northern India (10 ± 5 Mm^{-1}) below 2 km altitude (Fig. 4e). The average SSA over Bhubaneswar up to 2 km was >0.9 and SSA showed a dip at 21.7°N, 85.16°E corresponding to a high b_{ext} of 139 Mm^{-1} (Fig. 4f). The b_{abs} and b_{ext} values at this region were two times higher compared to the values over Bhubaneswar below 2 km altitude. Several fire

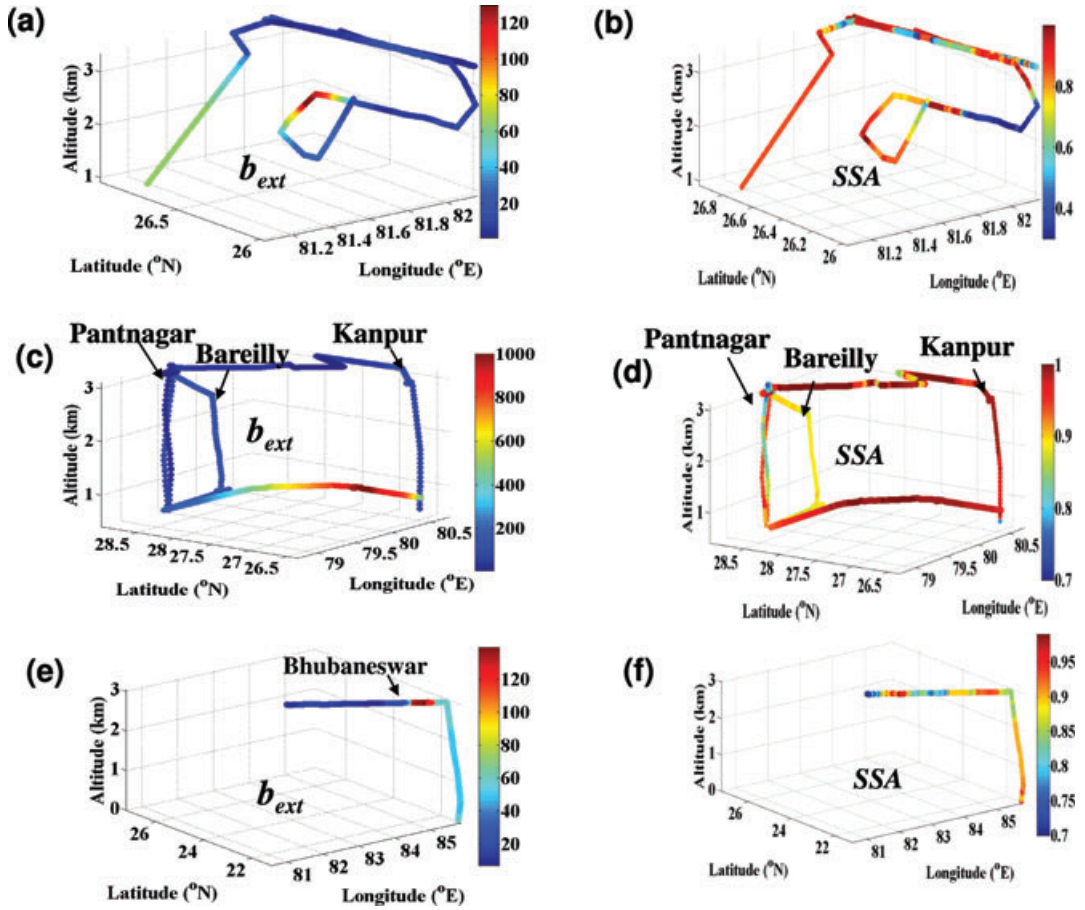

Fig. 4. (a) b_{ext} and (b) SSA over Kanpur on May 31, (c) b_{ext} and (d) SSA from Kanpur to Himalayan foothills on 30 May and (e) b_{ext} and (f) SSA from Kanpur to Bhubaneswar on 29 May. Colour bars (please note the difference in scale) in (a) to (f) show the respective optical parameter where b_{ext} is given in Mm^{-1}.

counts existed exactly over that point during sampling period as seen from MODIS. Close proximity to thermal power stations and coal fields (Fig. 1) and other industries near 23.77°N, 82.61°E (Chirimiri, Chhattisgarh, India) led to relatively higher b_{abs} and lower SSA.

4.2. *Aerosol characteristics during monsoon*

4.2.1. IG Plains to Himalayan foothills. Measurements were carried out over IG Plains covering three polluted cities Kanpur [forenoon (FN) and afternoon (AN) of 4 September], Delhi (5 September) and Chandigarh (10 September), with multilevel profiling over Kanpur at eight levels between 0.45 and 4 km above mean sea level (msl; Fig. 5). Kanpur to Delhi and Chandigarh (Figs 6a–d) and return were covered as bi-level sorties with vertical profiling up to 3 km over Delhi and Chandigarh. The AOD over Kanpur on 4 September was 0.31, which lies within the mean seasonal (monsoon) AOD ($\pm 1\sigma$) of 0.41 $\pm$ 0.29 implying that the aerosol characteristics on 4 September represent the entire seasonal characteristics.

An elevated aerosol layer (b_{ext} ~1500 Mm^{-1}) seen over Kanpur in the forenoon (FN) at 1.2 km disappeared with the evolution of boundary layer in the afternoon (AN). b_{ext} over Delhi showed similar peak between 1.5 and 2.6 km. Over Kanpur, the two peaks in M_F and b_{abs} in FN were shifted to higher altitudes in the AN indicating the role of thermal convection in dispersal of pollutants (Figure not shown). The peak in b_{abs} over Delhi and Kanpur had similar magnitude (30 Mm^{-1}) but the layer over Delhi was about 0.5 km higher than Kanpur. Higher b_{abs} (>10 Mm^{-1}) and lower SSA (~0.9) over polluted places between Kanpur and Aligarh were seen both below and above the boundary layer signifying the effects of local pollution.

Aerosols were extremely absorbing (SSA ~ 0.7) above 2 km and scattering (SSA > 0.9) below 2 km over Kanpur. A reversal in vertical gradients of M_F and b_{abs} at 3 km altitude with higher b_{abs} and lower M_F relative to low altitude further indicates that coarse mode particles play significant role in absorption above the boundary layer over Kanpur (Figure not shown). The b_{ext} values over Delhi were two to three times higher than Kanpur

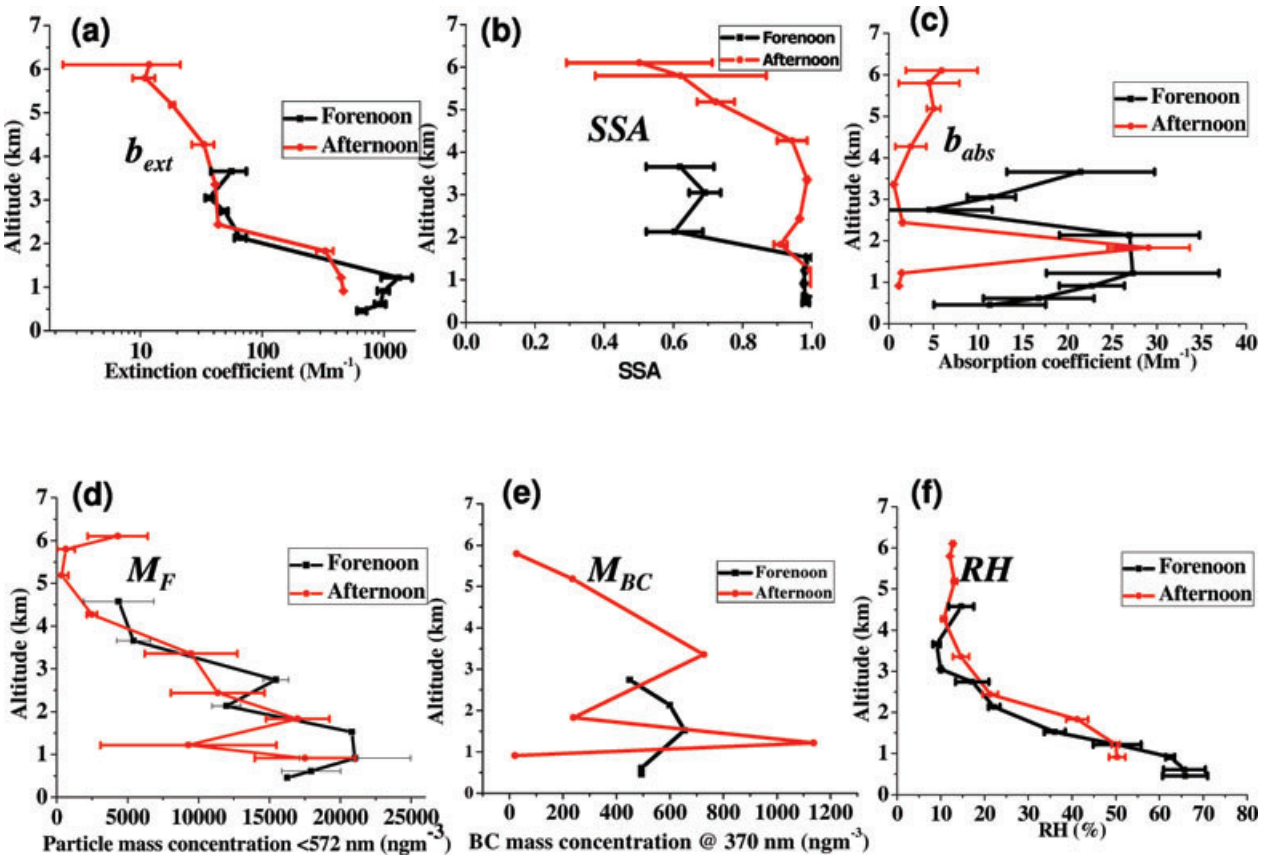

Fig. 5. (a) b_{ext}, (b) SSA, (c) b_{abs}, (d) F_{BC}, (e) M_F and (f) RH profiles over Kanpur in the FN and AN on 4 September. *x*- and *y*-axes represent the respective parameters and altitude in km.

and Lucknow at similar altitudes, which could be due to higher aerosol concentration, but the observations may be affected by high RH (70%). An elevated absorbing layer ($b_{abs} \sim 35$ Mm^{-1}) with low SSA (~0.9) is seen at 2.5 km over Aligarh with three to four times higher b_{abs} compared to the nearby rural areas which can be taken as the background (Figs 6b and d). Such a large variability in 3-D distribution of particle properties must be accounted in regional climate models to reduce the uncertainty of aerosol forcing.

A heavy thunderstorm till 0500 h IST on 10 September over Kanpur cleaned the atmosphere by wet deposition thereby reducing the b_{ext} and b_{scat} values by two to four times than 4, 5 and 9 September (Fig. 6c). During descend, b_{abs} (~25 Mm^{-1}) shows values similar to the pre-monsoon values when RH < 50%. The b_{abs} during ascend was not considered as the RH was >50% which can lead to underestimation of b_{abs}. The b_{abs} similar to pre-monsoon indicates faster build-up of absorbing aerosols compared to scattering aerosols, because scattering aerosols (e.g. sulphate) may take longer time to form and rebuild than absorbing (EC/soot) aerosols.

Figures 6e and f show the variations of optical properties of aerosols during the monsoon season from IG Plains to Himalayan foothills. Unlike the pre-monsoon season, b_{ext} within the boundary layer was higher near the foothills than the IG Plains which could be due to higher RH (>50%) in the foothills. Because the trend was opposite to that found in pre-monsoon, the role of local emissions in the increase of b_{ext} over foothills was ruled out.

4.2.2. IG Plains—the Great Indian Desert, Coastal and Central India. Measurements were carried out from IG Plains to the Great Indian Desert on 11 September. b_{abs} over urban cities such as Lucknow and Agra showed peaks at 3 km indicating high loading of absorbing aerosols due to local pollution. Coarse mode particles showed dominance at 3 km over Agra and Kanpur increasing the b_{ext} aloft.

Vertical and spatial profiling of aerosol properties over central and coastal India were carried out on 14 and 15 September. b_{abs} peaked up near Korba and Chirimiri coal fields similar to pre-monsoon season. The b_{ext} over central and coastal India are comparable to Desert and Himalayan foothills at 3 km (Appendix S2).

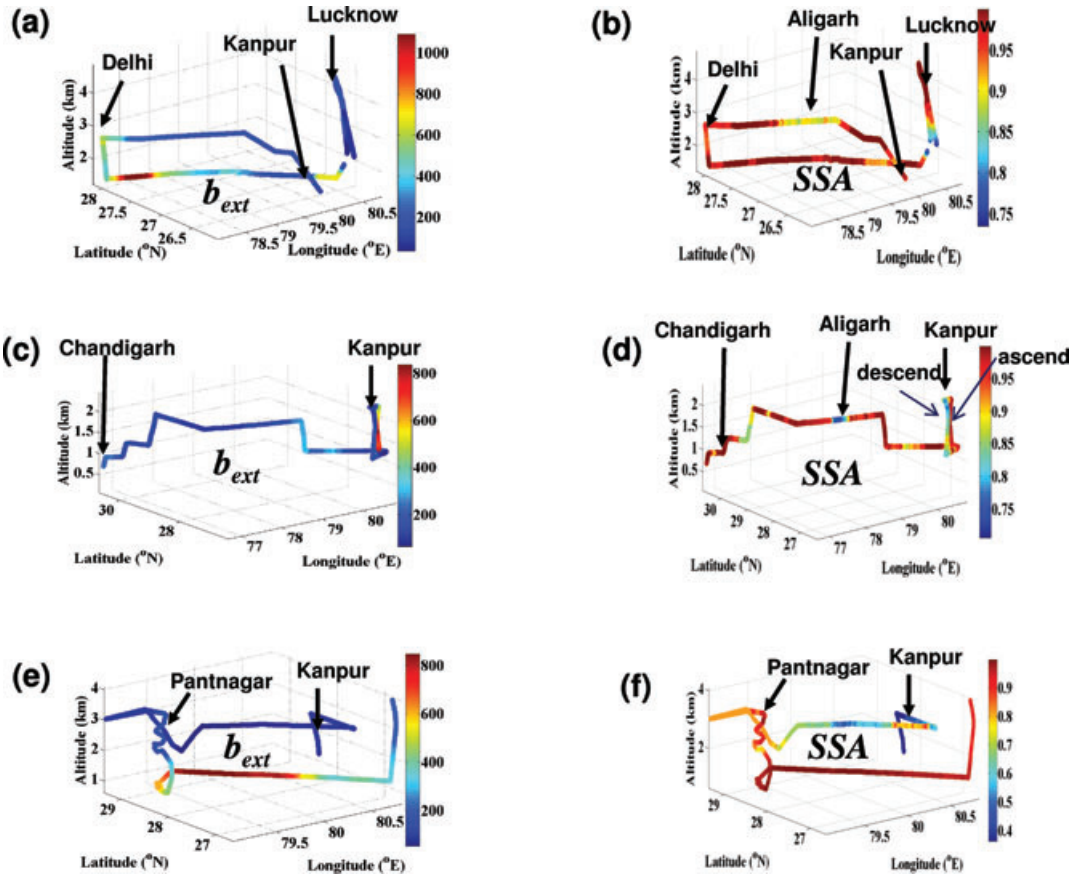

Fig. 6. (a) b_{ext} and (b) SSA from Kanpur to Delhi on 5 September, (c) b_{ext} and (d) SSA from Kanpur to Chandigarh on 10 September and (e) b_{ext} and (f) SSA from Kanpur to Himalayan foothills on 9 September. *x*- and *y*-axes represent the latitude and longitude and *z*-axis has the height. Colour bars in (a) to (f) show the respective optical parameter. b_{ext} is given in Mm^{-1}.

4.3. Scale heights at locations with vertical profiling

Scale heights derived from exponentially decreasing b_{ext} profiles are expressed by the exponential equation:

$$b_{ext,a} = b_{ext,o} \exp(-z/H_{aer}), \quad (5)$$

where H_{aer} is the scale height at which b_{ext} decrease by a factor $(1/e)$. All the data points inside the clouds and at high RH were carefully removed for the analysis. The profile for May 31 showing an elevated layer at about 2 km did not follow an exponentially decreasing/increasing profile on that day due to which scale height could not be calculated. For similar reasons, scale height was not calculated over Pantnagar and Bareilly during pre-monsoon.

Exponentially decreasing b_{ext} values with a scale height of 0.25 km were observed between 1.2 and 3.6 km in the FN over Kanpur during monsoon indicating confinement of aerosols at lower altitudes. But b_{ext} values increased exponentially up to 1.2 km with a negative scale height of −1.42 km. In the AN, the scale height was 1.25 up to 2.4 km altitude and 3.06 km above that up to a height of 6 km indicating the spread of aerosol with height as the boundary layer is established. The scale height over Pantnagar in the AN was calculated between 1 and 3 km altitude, which came out to be 1.43 km that is similar to Kanpur in the AN. The scale heights are tabulated in Table 3, which shows similar scale heights over IG Plains (1.25 km for Kanpur and 1.43 km for Pantnagar) after the buildup of boundary layer but this needs validation with more data. b_{ext} profile over Bhubaneswar on 14 September yielded a scale height of 1.82 km from 1.2 to 2.8 km altitude, which is slightly higher than Himalayan foothills. Scale height for central India could not be calculated due to the presence of clouds.

4.4. 3-D views of aerosol radiative properties

The 3-D distribution of aerosols in the pre-monsoon season is shown in Figs 7a and b by interpolating the measured data at 1 and 3 km altitudes. If more than one value existed at a particular point due to multiple measurements on different days, the average value was used during interpolation. Highest b_{ext} were seen over IG Plains and Himalayan foothills, whereas central and coastal India showed lower values at 1 km. Jaipur showed relatively higher values of b_{ext} at both altitudes due to the higher

Table 3. *Scale heights at different locations*

Location	Season	Altitude range (km)	Scale height (km)	Remarks
Kanpur (September 4) FN	Monsoon	< 1.2km	−1.42	Elevated layer up to 1.2 km. b_{ext} increased with altitude
		1.2–4	0.25	
Kanpur (September 4) AN	Monsoon	0.9–2.4	1.25	
		2.4–6.1	3.06	
Bhubaneswar (September 14)	Monsoon	1.2–2.8	1.82	
Pantnagar (September 9)	Monsoon	1.0–3.0	1.43	

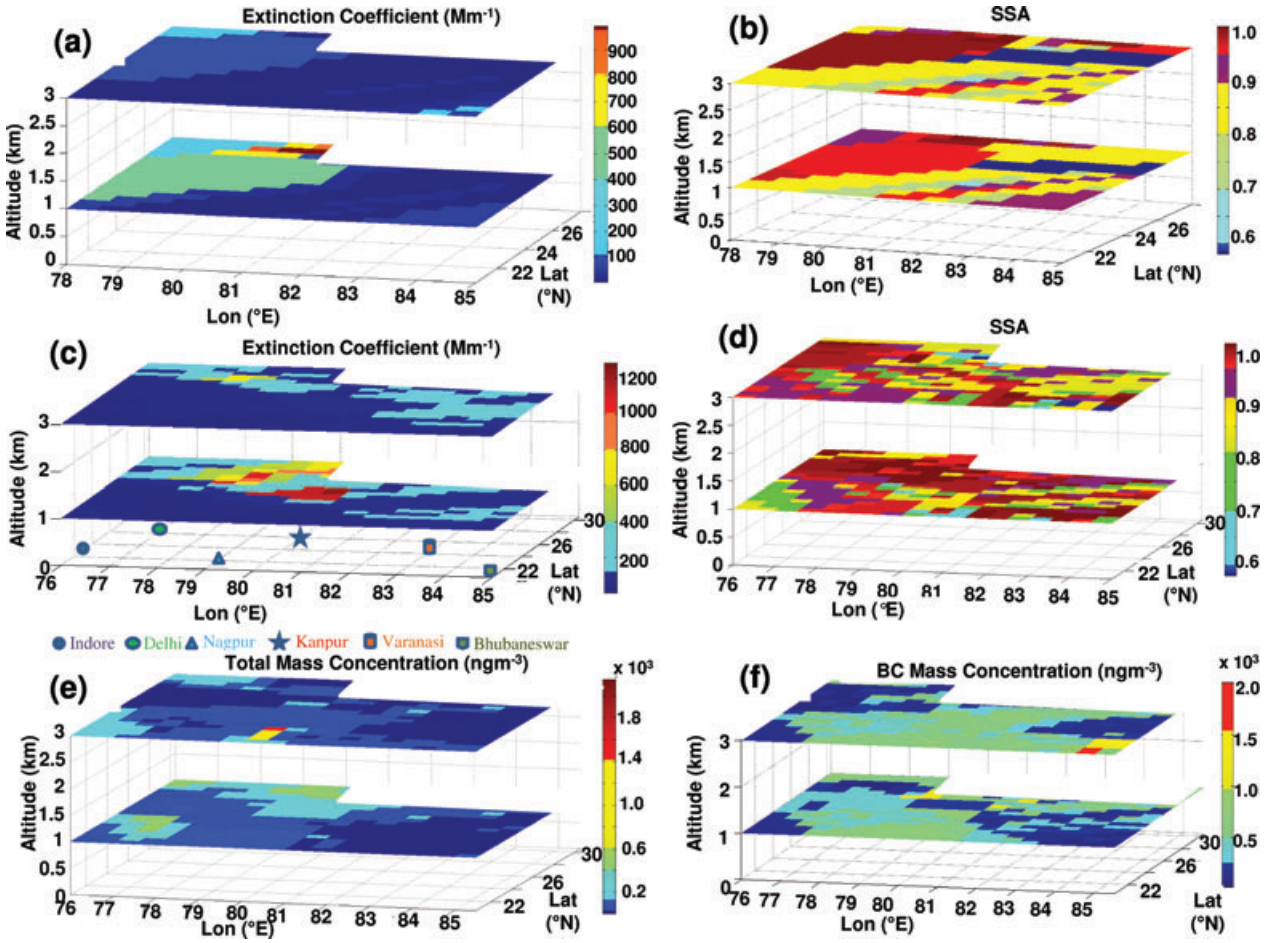

Fig. 7. Summary plot (a) b_{ext} and (b) SSA for pre-monsoon and (c) b_{ext}, (d) SSA, (e) M_T and (f) M_{BC} for monsoon season. Latitude and longitude are abbreviated as Lat and Lon, respectively.

loading of dust aerosols relative to central and coastal India. Thus, a distinct longitudinal gradient in b_{ext} can be seen at both the altitudes with higher values towards the west and lower towards the east of CTCZ. Similarly, b_{ext} increased with latitude in the CTCZ at both 1 and 3 km altitude. SSA showed largely low values suggesting dominance of absorbing aerosols both at 1 km and at 3 km except over Jaipur and Himalayan foothills. No gradient was seen in SSA in terms of latitude and longitude, except for highly absorbing aerosols in the central India. During the pre-monsoon, measurements of aerosol optical properties were not carried out over Desert and central India due to technical problems.

Figures 7c–f show a summary plot of b_{ext}, SSA, M_T and M_{BC} over the entire CTCZ region showing higher aerosol loading at both the altitudes over IG Plains, Desert and Himalayan foothills and central and coastal India show relatively cleaner conditions

Table 4. *Optical properties of aerosols at different height ranges over different regions during pre-monsoon and monsoon seasons*

Location	Altitude range (km)	Extinction coefficient (Mm^{-1})	SSA	Total mass (μgm^{-3})
Pre-monsoon				
Kanpur (May 30)	1–2	93.78 ± 0.82	0.96	NA
	2–3	95.15 ± 1.49	0.96	NA
Pantnagar (May 30)	<1	70.29 ± 15.33	0.92	NA
	1–2	63.96 ± 34.60	0.88	NA
	2–3	59.67 ± 35.61	0.87	NA
Bareilly (May 30)	1–2	144.39 ± 0.89	0.89	NA
	2–3	143.62 ± 0.79	0.89	NA
Bhubaneswar (May 29)	<1	50.28 ± 3.68	0.91	NA
	1–2	43.72 ± 1.03	0.90	NA
	2–3	48.53 ± 4.62	0.87	NA
Monsoon				
Kanpur (September 4) FN	<1	919.68 ± 134.28	0.98	NA
	1–2	672.32 ± 610.76	0.98	NA
	2–3	49.73 ± 10.26	0.79	NA
Pantnagar (September 9)	<1	481.25 ± 25.35	0.97	44 ± 2.4
	1–2	233.92 ± 86.57	0.88	19.3 ± 1.1
	2–3	157.05 ± 11.46	0.91	12.4 ± 2.0
Nainital (September 9)	3	91.01 ± 2.85	0.83	8.3 ± 0.4
Bhubaneswar (September 14)	1–2	57.46 ± 1.5	0.60	9 ± 2.8
	2–3	27.75 ± 5.17	0.95	5.8 ± 0.3
Indore (September 14)	<1	24.64 ± 2.68	0.78	11 ± 0.02
	1–2	22.95 ± 9.33	0.84	29 ± 20
	2–3	17.46 ± 1.4	0.97	50 ± 29
Jaipur (September 11)	1–2	190.25 ± 78.66	0.97	7.5 ± 5.5
	2–3	74.41 ± 38.19	0.95	1.8 ± 0.19
Chandigarh (September 10)	<1	205.69 ± 6.25	0.97	48.7 ± 5.7
	1–2	140.24 ± 37.23	0.92	27 ± 0.46
Delhi (September 5)	1–2	457.64 ± 17.04	0.98	NA
	2–3	548.73 ± 44.21	0.94	NA

which is in correspondence with M_T. Highly absorbing layer at 3 km was evident over CTCZ except over desert. M_{BC} shows nearly uniform concentrations at both the altitudes except high values over Bhubaneswar at 3 km due to fire count and over Kanpur at 1 km. Higher b_{ext} and M_T were seen over northern (IG Plains, Himalayan foothills) than the central and coastal CTCZ at 1 km. No longitudinal variation in b_{ext} was seen during the monsoon. High M_{BC} was seen over the entire CTCZ at both altitudes with notably high concentration (500–1000 ngm^{-3}) over central India and IG Plains.

The aerosol optical and mass properties during the monsoon season are summarized in Table 4. The b_{ext} over IG Plains and Himalayan foothills during the monsoon were much higher than the pre-monsoon season below 2 km altitude, but show a sharp decrease aloft. Precipitation reduced b_{ext} by ∼50%, but the b_{abs} resumed to 25 Mm^{-1} within 3 h. Elevated layers were also seen during monsoon as indicated by M_F, M_T and b_{ext} profiles over IG Plains, Desert and Central India.

5. Aerosol heating rate

HR in an aerosol–laden atmosphere depends on optical properties of aerosols and their vertical distribution, solar zenith angle, surface albedo and atmospheric conditions (e.g. clear or cloudy). The results of diurnal HR in clear sky for pre-monsoon and monsoon season were calculated and discussed as under.

5.1. Pre-monsoon season

IG Plains has the highest loading in the pre-monsoon season contributed by local anthropogenic aerosols and transported mineral aerosols (Singh et al., 2004; Gautam et al., 2007). Kanpur (IG Plains) shows higher HR at different levels compared to other locations for both pre-monsoon and monsoon seasons (Figs 8a and b). During the pre-monsoon season over Kanpur, the peak HR of 0.8 K day^{-1} was observed at 2.1 km, which coincides with the peak in b_{abs}. The diurnal top of the atmosphere (TOA) and

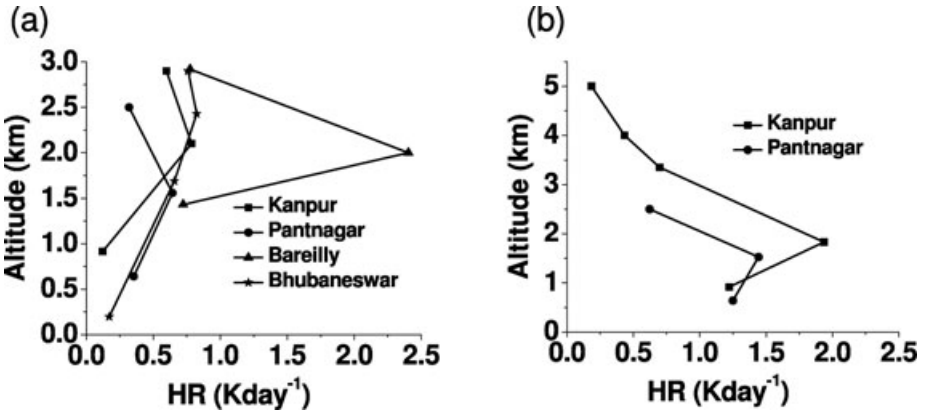

Fig. 8. Combined HR profiles during (a) pre-monsoon and (b) monsoon.

surface forcings were −20.3 and −50.2 Wm^{-2}, respectively. These values are comparable with the values estimated over Kanpur from 2001 to 2005, although the present profiling location is 200 km away from Kanpur city where the AERONET measurements from 2001 to 2005 were carried out (Dey and Tripathi, 2008). In this study, the TOA and surface forcing are estimated by giving the vertical profiles of aerosols as input. It should be noted that these vertical profiles do not affect the TOA and surface forcing (Ramachandran and Kedia, 2010). Tripathi et al. (2007) calculated the HR profiles from surface to about 1.5 km during pre-monsoon (June 2005) and found that the HR increased with height in the AN up to 1.75 K day^{-1} at 1.2 km. In Tripathi et al. (2007), calculations were constrained by M_{BC}, M_T, and AOD, whereas in this study, b_{ext}, b_{abs}, SSA and M_{BC} were constrained spectrally. Because the methodology is similar, the difference in HR values may be attributed to different aerosol properties in two different years as the F_{BC} was 17% in 2005 and SSA was <0.7 (M_{BC} and M_T is not available for pre-monsoon to calculate F_{BC}) during this study indicating more absorbing fraction of aerosols. When fires contribute to the loading as in Bareilly during the pre-monsoon season which increases the proportion of absorbing aerosols thereby reducing the SSA below 0.95, the HR profile showed high HR values up to ∼2.5 K day^{-1}. A peak with such a higher HR can lead to boundary layer inversion thus, inhibiting the vertical transport of aerosols (Tripathi et al., 2007). The TOA and surface forcing over Bareilly were −27.6 and −80.57 Wm^{-2}. Absorbing aerosols, therefore, highly governs the HR profile of Kanpur as also seen in Tripathi et al. (2007) and Li et al. (2007). Gautam et al. (2010) using satellite (CALIPSO, CERES) and ground-based (AERONET) observations and 1-D delta-four-stream radiative transfer program estimated the radiative HR for the aerosol laden atmosphere during the pre-monsoon season for a period of 2 years. The daily average HR over IG Plains peaked around 3 km to a value near 2 K day^{-1}. The spatial difference might have led to the observed difference in HR. The profiles look similar even though Gautam et al. (2010) showed the average of entire IG Plains. Kuhlmann and Quaas (2010) used only satellite (CALIPSO) observations and calculated the HR during pre-monsoon seasons for three consecutive years (2006–2008). The peaks in HR in their study lied between 2 and 3 km over Gangetic plains but the peak value was around 0.35 K day^{-1}. The use of in situ data to calculate the optical properties could have led to high diurnally averaged HR than those given Kuhlmann and Quaas (2010) whereas lesser than in Gautam et al. (2010) as their computations were on few years data against few days in this study, thus justifies the need for in situ measurements to constrain the OPAC model.

HR over the Himalayan foothills followed the b_{abs} profiles. The maximum value of HR at Pantnagar was 0.64 K day^{-1}, which is comparable to Kanpur and Bhubaneswar. Lower aerosol concentrations in the lower layers and low b_{ext} have led to low values of HR. HR has been evaluated in the foothills of central Himalayas (Pantnagar) at lower altitudes for the first time to the best of authors' knowledge. Gautam et al. (2009b) studied the vertical extent of aerosol piling against the Himalayan slopes during the pre-monsoon season using CALIPSO images. They found instantaneous HR in IG Plains of ∼6.5 K day^{-1} at 3.5 km over the region which extended up to mid-troposphere and results in enhanced HR (4.5–2 K day^{-1}) in the 4–7 km altitude range which was missed during the current experiment. The TOA and surface forcing over Pantnagar were −22.1 and −44.7 Wm^{-2}, respectively. Ramana et al. (2004) estimated the TOA and surface forcing over Himalayas as 0 and −25 Wm^{-2}.

Bhubaneswar during the pre-monsoon season, when high proportion of absorbing aerosols contributed by fire counts reduce the SSA to < 0.95, the HR profile closely followed the b_{abs} profile with peak HR value of 0.8 K day^{-1} at 2.43 km. Moorthy et al. (2009) studied the vertical profiles of aerosol properties over Bhubaneswar using LIDAR and in situ measurements during March 2006. They found TOA and surface forcings of −20 and −50.6 Wm^{-2}, respectively whereas in this study those were −19.5 and −48.4 Wm^{-2}, respectively. The vertical profile of HR with MPL and in situ measurements closely matches with the present study indicating that the aerosol distribution and loading

in the atmosphere remained similar in the pre-monsoon of 2006 and 2008. Satheesh et al. (2008) studied the aerosol vertical profiles of b_{ext} using Micro Pulse Lidar over central and southern India during the pre-monsoon season of 2006 and found a warming of $\sim$1.5 K day^{-1} above 3 km.

Peaks in HR occurred at about 1.5 km in Pantnagar, $\sim$2.1 km in Kanpur, $\sim$2.1 km in Bareilly and 2.5 km in Bhubaneswar even though the absolute value at peaks over Bareilly is $>$2.5 times higher than other locations studied. No latitudinal gradient is seen in terms of HR up to 3 km during the pre-monsoon season.

5.2. Monsoon season

During monsoon, due to the presence of clouds, spectral AOD was not available for all the locations where vertical profiling was available. The spectral AOD from AERONET/MODIS was available for only two locations—Kanpur and Pantnagar where the sky was clear over the AERONET site on the day of experiment. The HR profiles over only these two locations are discussed in this section.

Kanpur is the only location in the IG basin where HR profile is available for the pre-monsoon season to study the inter-seasonal variation in HR. During the monsoon season, the vertical profiling was carried out over Kanpur city unlike in pre-monsoon season. It was found that the HR values showed a peak around 1.8 km coinciding with the peak in b_{abs} values. These values were higher than the pre-monsoon values when compared altitude-wise. There are three reasons behind this. First, the locations were spatially apart, the pre-monsoon profiling was carried out over a rural agricultural area whereas the monsoon profiling was carried out over urban area. Secondly, the quick buildup of aerosols after the rain brings the aerosol loading similar to the pre-monsoon season. Thirdly, the aerosol loading over urban Kanpur is comparable to that of Bareilly. Thus, the HR values over Kanpur in the monsoon are slightly less than Bareilly, while the TOA and surface forcings being comparable.

Over the Himalayan foothills, in Pantnagar, the HR profile closely followed the b_{ext} profile and also the values were lesser than Kanpur for the seasons. Although b_{abs} showed a peak at 1.8 km in the monsoon, the SSA was above 0.95 showing the dominance of scattering aerosols.

5.3. Implications to regional climate

Aerosols absorb direct and reflected solar radiation thereby reducing the radiation reaching the Earth's surface (Ramanathan et al., 2001) known as surface dimming. This surface dimming, which is evident from the large negative surface forcings over entire CTCZ region particularly over urban locations such as Bareilly, can lead to reduction in surface evaporation by decreasing either or both of latent heat flux and sensible heat flux. The high diurnal HR values up to 3 km as seen over CTCZ will increase the stability of lower troposphere thus inhibiting the convection process. This positive feedback will allow more build up of aerosols and adversely affect air quality and hydrological cycle.

6. Summary and conclusions

CTCZ experiment is the first attempt to get the 3-D variability of optical and physical properties of aerosols over the Indian CTCZ region during the pre-monsoon and monsoon seasons. HR over the entire CTCZ region were calculated from real-time b_{abs}, b_{scat} and M_T profiles at different levels that reduces the uncertainty as compared to any previous estimates (e.g. Tripathi et al., 2007). The following major conclusions are drawn from the results.

1. Higher aerosol loading over IG Plains and Himalayan foothills against cleaner conditions in central and coastal India was seen during pre-monsoon season.
2. Highly absorbing aerosols corresponding to SSA $<$ 0.9 and persistent elevated layers were found over IG Plains and Himalayan foothills where more than 50% of AOD were contributed from aerosols, mostly dust, above 4 km, whereas relatively cleaner conditions existed over coastal India during the pre-monsoon. The b_{abs} over coastal India were a third of that observed in IG Plains and Himalayan foothills.
3. The absorbing aerosols rebuild faster in the atmosphere after the washout of aerosols by rain compared to scattering aerosols. Elevated aerosol layers were evident during the monsoon as well.
4. The diurnal HR values were higher in urban regions of IG Plains at all altitudes in CTCZ during both the seasons. IG Plains showed higher HR than other regions of CTCZ with the peak value as high as 2.5 K day^{-1}.

7. Acknowledgments

This work was financially supported by DST ICRP and ISRO GBP Programmes. We acknowledge the entire aircraft crew, NRSC, Department of Space for their help in organizing scientific flights. We thank the site manager and staffs for their effort in maintaining the Kanpur, Bareilly and Pantnagar AERONET sites. NCEP Image was provided by the NOAA/ESRL Physical Sciences Division, Boulder, Colorado. CALIPSO image was provided by NASA Langley Research Center Atmospheric Science Data Center. Sagnik Dey acknowledges research grant from IIT-Delhi under contract IITD/IRD/MI00769.

References

Abrol, Y. P., Sangwan, S. and Tiwari, M. K. 2002. *Land Use—Historical Perspectives, Focus on Indo-Gangetic Plains*. Allied Publishers Pvt. Ltd., New Delhi.

Ackerman, A. S., Toon, O. B., Taylor, J. P., Johnson, D. W., Hobbs, P. V. and co-authors. 2000. Effects of aerosols on cloud albedo:

evaluation of Twomey's parameterization of cloud susceptibility using measurements of ship tracks. *J. Atmos. Sci.* **57**, 2684–2695.

Albrecht, B. A. 1989. Aerosols, cloud microphysics, and fractional cloudiness. *Science* **245**, 1227–1230.

Arnott, W. P., Moosmuller, H., Rogers, C. F., Jin, T. F. and Bruch, R. 1999. Photoacoustic spectrometer for measuring light absorption by aerosol: instrument description. *Atmos. Environ.* **33**, 2845–2852.

Arnott, W. P., Moosmuller, H., Sheridan, P. J., Ogren, J. A., Raspet, R. and co-authors. 2003. Photoacoustic and filter-based ambient aerosol light absorption measurements: instrument comparisons and the role of relative humidity. *J. Geophys. Res.-Atmos.* **108**, 4034, doi:10.1029/2002JD002165.

Arnott, W. P., Walker, J. W., Moosmuller, H., Elleman, R. A., Jonsson, H. H. and co-authors. 2006. Photoacoustic insight for aerosol light absorption aloft from meteorological aircraft and comparison with particle soot absorption photometer measurements: DOE Southern Great Plains climate research facility and the coastal stratocumulus imposed perturbation experiments. *J. Geophys. Res.-Atmos.* **111**, D05S02, doi:10.1029/2005JD005964.

Babu, S. S. and Moorthy, K. K. 2002. Aerosol black carbon over a tropical coastal station in India. *Geophys. Res. Lett.* **29**, 2098, doi: 10.1029/2002GL05662.

Babu, S. S., Satheesh, S. K., Moorthy, K. K., Dutt, C. B. S., Nair, V. S. and co-authors. 2008. Aircraft measurements of aerosol black carbon from a coastal location in the north-east part of peninsular India during ICARB. *J. Earth Sys. Sci.* **117**, 263–271.

Baron, P. A. and Willeke, K. 2001. *Aerosol Measurements: Principles, Techniques and Applications*. Wiley, New York.

Beegum, S. N., Moorthy, K. K., Babu, S. S., Satheesh, S. K., Vinoj, V. and co-authors. 2009. Spatial distribution of aerosol black carbon over India during pre-monsoon season. *Atmos. Environ.* **43**, 1071–1078.

Chand, D., Wood, R., Anderson, T. L., Satheesh, S. K. and Charlson, R. J. 2009. Satellite-derived direct radiative effect of aerosols dependent on cloud cover. *Nat. Geosci.* **2**, 181–184.

Chinnam, N., Dey, S., Tripathi, S. N. and Sharma, M. 2006. Dust events in Kanpur, northern India: chemical evidence for source and implications to radiative forcing. *Geophys. Res. Lett.* **33**, L08803, doi:10.1029/2005GL025278.

CTCZ science plan. 2008. *Indian Climate Research Programme*. Govt. of India, Ministry of Science and Technology, India

Corrigan, C. E., Roberts, G. C., Ramana, M. V., Kim, D. and Ramanathan, V. 2008. Capturing vertical profiles of aerosols and black carbon over the Indian Ocean using autonomous unmanned aerial vehicles. *Atm. Chem. Phys. Discuss.* **8**, 737–747.

Das, N., Baral, S. S., Sahoo, S. K., Mohapatra, R. K., Ramulu, T. S. and co-authors. 2009. Aerosol physical characteristics at Bhubaneswar, East coast of India. *Atmos. Res.* **93**, 897–901.

Davies, D. K., Ilavajhala, S., Min Minnie, W. and Justice, C. O. 2009. Fire information for resource management system: archiving and distributing MODIS Active Fire Data. *IEEE Trans. Geosci. Remote Sens.* **47**, 72–79.

Dey, S. and Di Girolamo, L. 2010. A climatology of aerosol optical and microphysical properties over the Indian subcontinent from 9 years (2000–2008) of Multiangle Imaging Spectroradiometer (MISR) data. *J. Geophys. Res.* **115**, D15204, doi:10.1029/2009JD013395.

Dey, S. and Tripathi, S. N. 2007. Estimation of aerosol optical properties and radiative effects in the Ganga basin, northern India, during the wintertime. *J. Geophys. Res.* **112**, D03203, doi:10.1029/2006JD007267.

Dey, S. and Tripathi, S. N. 2008. Aerosol direct radiative effects over Kanpur in the Indo-Gangetic basin, northern India: long-term (2001–2005) observations and implications to regional climate. *J. Geophys. Res.- Atm.* **113**, D04212.

Dey, S., Tripathi, S. N., Singh, R. P. and Holben, B. N. 2004. Influence of dust storms on the aerosol optical properties over the Indo-Gangetic basin. *J. Geophys. Res.* **109**, D20211, doi:10.1029/2004JD004924.

Dey, S., Tripathi, S. N. and Mishra, S. K. 2008. Probable mixing state of aerosols in the Indo-Gangetic Basin, northern India. *Geophys. Res. Lett.* **35**, L03808, doi:10.1029/2007GL032622.

Draxler, R. R. and Hess, G. D. 1998. An overview of the HYSPLIT_4 modeling system of trajectories, dispersion, and deposition. *Aust. Meteor. Mag.*, **47**, 295–308.

Draxler, R. R. and Rolph, G. D. 2011. HYSPLIT (HYbrid Single-Particle Lagrangian Integrated Trajectory) model access via NOAA ARL READY Website (http://ready.arl.noaa.gov/HYSPLIT.php). NOAA Air Resources Laboratory, Silver Spring, MD.

Dumka, U. C., Moorthy, K. K., Pant, P., Hegde, P., Sagar, R. and co-authors. 2008. Physical and optical characteristics of atmospheric aerosols during ICARB at Manora Peak, Nainital: a sparsely inhabited, high-altitude location in the Himalayas. *J. Earth Sys. Sci.* **117**, 399–405.

Fierz-Schmidhauser, R., Zieger, P., Wehrle, G., Jefferson, A., Ogren, J. A. and co-authors. 2009. Measurement of relative humidity dependent light scattering of aerosols. *Atmos. Meas. Tech.* **3**, 39–50.

Ganguly, D., Gadhavi, H., Jayaraman, A., Rajesh, T. A. and Misra, A. 2005. Single scattering albedo of aerosols over the central India: Implications for the regional aerosol radiative forcing. *Geophys. Res. Lett.* **32**, L18803, doi:10.1029/2005GL023903.

Ganguly, D., Ginoux, P., Ramaswamy, V., Winker, D. M., Holben, B. N. and co-authors. 2009. Retrieving the composition and concentration of aerosols over the Indo-Gangetic basin using CALIOP and AERONET data. *Geophys. Res. Lett.* **36**, L13806, doi: 10.1029/2009GL038315.

Gautam, R., Hsu, N. C., Kafatos, M. and Tsay, S. C. 2007. Influences of winter haze on fog/low cloud over the Indo-Gangetic plains. *J. Geophys. Res.* **112**, D05207, doi: 10.1029/2005JD007036.

Gautam, R., Hsu, N. C., Lau, K. M. and Kafatos, M. 2009a. Aerosol and rainfall variability over the Indian monsoon region: distributions, trends and coupling. *Annal. Geophys.* **27**, 3691–3703.

Gautam, R., Hsu, N. C., Lau, K. M., Tsay, S. C. and Kafatos, M. 2009b. Enhanced pre-monsoon warming over the Himalayan-Gangetic region from 1979 to 2007. *Geophys. Res. Lett.* **36**, L07704, doi: 10.1029/2009GL037641.

Gautam, R., Hsu, N. C. and Lau, K. M. 2010. Premonsoon aerosol characterization and radiative effects over the Indo-Gangetic Plains: implications for regional climate warming. *J. Geophys. Res.* **115**, D17208, doi:10.1029/2010JD013819.

Good, N., Coe, H. and McFiggans, G. 2010. Instrumentational operation and analytical methodology for the reconciliation of aerosol water uptake under sub- and supersaturated conditions. *Atmos. Meas. Tech.* **3**, 1241–1254.

Hahn, D. G. and Manabe, S. 1975. Role of mountains in south Asian monsoon circulation. *J. Atmos. Sci.* **32**, 1515–1541.

Hess, M., Koepke, P. and Schult, I. 1998. Optical properties of aerosols and clouds: the software package OPAC. *Bull. Am. Meteorol. Soc.* **79**, 831–844.

IPCC. 2007. *Climate Change 2007: The Physical Science Basis*. Cambridge University Press, Cambridge.

Jethva, H., Satheesh, S. K., Srinivasan, J. and Moorthy, K. K. 2009. How good is the assumption about visible surface reflectance in MODIS aerosol retrieval over land? A comparison with aircraft measurements over an urban site in India. *IEEE Trans. Geosci. Remote Sens.* **47**, 1990–1998.

Kahn, R. A., Nelson, D. L., Garay, M. J., Levy, R. C., Bull, M. A. and co-authors. 2009. MISR aerosol product attributes and statistical comparisons with MODIS. *IEEE Trans. Geosci. Remote Sens.* **47**, 4095–4114.

Kalnay, E., Kanamitsu, M., Kistler, R., Collins, W., Deaven, D. and co-authors. 1996. The NCEP/NCAR 40-year reanalysis project. *Bull. Amer. Meteor. Soc.* **77**, 437–471.

Kuhlmann, J. and Quaas, J. 2010. How can aerosols affect the Asian summer monsoon? Assessment during three consecutive pre-monsoon seasons from CALIPSO satellite data. *Atmos. Chem. Phys. Discuss.* **10**, 4673–4688.

Lau, K. M., Kim, M. K. and Kim, K. M. 2006. Asian summer monsoon anomalies induced by aerosol direct forcing: the role of the Tibetan Plateau. *Clim. Dynam.* **26**, 855–864.

Lewis, K., Arnott, W. P., Moosmuller, H. and Wold, C. E. 2008. Strong spectral variation of biomass smoke light absorption and single scattering albedo observed with a novel dual-wavelength photoacoustic instrument. *J. Geophys. Res.- Atmos.* **113**, D16203, doi: 10.1029/2007JD009699.

Lewis, K. A., Arnott, W. P., Moosmuller, H., Chakrabarty, R. K., Carrico, C. M. and co-authors. 2009. Reduction in biomass burning aerosol light absorption upon humidification: roles of inorganically-induced hygroscopicity, particle collapse, and photoacoustic heat and mass transfer. *Atmos. Chem. Phys.* **9**, 8949–8966.

Li, Z. Q., Xia, X. G., Cribb, M. R., Mi, W., Holben, B. and co-authors. 2007. Aerosol optical properties and their radiative effects in northern China. *J. Geophys. Res.- Atmos.* **112**, D22S01, doi: 10.1029/2006JD007382.

Mahowald, N. M. and Dufresne, J. L. 2004. Sensitivity of TOMS aerosol index to boundary layer height: implications for detection of mineral aerosol sources. *Geophys. Res. Lett.* **31**, L03103, doi:10.1029/2003GL018865.

McMurry, P. H., Wang, X., Park, K. and Ehara, K. 2002. The relationship between mass and mobility for atmospheric particles: a new technique for measuring particle density. *Aerosol Sci. Technol.* **36**, 227–238.

Mishra, S. K. and Tripathi, S. N. 2008. Modeling optical properties of mineral dust over the Indian Desert. *J. Geophys. Res.- Atmos.* **113**, D23201, doi: 10.1029/2008JD010048.

Mishra, S. K., Dey, S. and Tripathi, S. N. 2009. Implications of particle composition and shape to dust radiative effect: a case study from the Great Indian Desert. *Geophys. Res. Lett.* **35**, L23814, doi:10.1029/2008GL036058.

Moorthy, K. K., Babu, S. S. and Satheesh, S. K. 2005. Aerosol characteristics and radiative impacts over the Arabian Sea during the intermonsoon season: results from ARMEX field campaign. *J. Atmos. Sci.* **62**, 192–206.

Moorthy, K. K., Nair, V. S., Babu, S. S. and Satheesh, S. K. 2009. Spatial and vertical heterogeneities in aerosol properties over oceanic regions around India: implications for radiative forcing. *Q. J. Roy. Meteor. Soc.* **135**, 2131–2145.

Murugavel, P., Gopalakrishnan, V., Pant, V. and Kamra, A. K. 2008. Airborne measurements of submicron aerosols across the coastline at Bhubaneswar during ICARB. *J. Earth Sys. Sci.* **117**, 273–280.

Nair, V. S., Moorthy, K. K., Alappattu, D. P., Kunhikrishnan, P. K., George, S. and co-authors. 2007. Wintertime aerosol characteristics over the Indo-Gangetic Plain (IGP): impacts of local boundary layer processes and long-range transport. *J. Geophys. Res.* **112**, D13205, doi:10.1029/2006JD008099.

Niranjan, K., Madhavan, B. L. and Sreekanth, V. 2007. Micro pulse lidar observation of high altitude aerosol layers at Visakhapatnam located on the east coast of India. *Geophys. Res. Lett.* **34**, L03815, doi: 10.1029/2006GL028199.

Pant, P., Hegde, P., Dumka, U. C., Sagar, R., Satheesh, S. K. and co-authors. 2006. Aerosol characteristics at a high-altitude location in central Himalayas: Optical properties and radiative forcing. *J. Geophys. Res.- Atmos.* **111**, D17206, doi: 10.1029/2005JD006768.

Prospero, J. M., Ginoux, P., Torres, O., Nicholson, S. E. and Gill, T. E. 2002. Environmental characterization of global sources of atmospheric soil dust identified with the Nimbus 7 Total Ozone Mapping Spectrometer (TOMS) absorbing aerosol product. *Rev. Geophys.* **40**, 1002, doi: 10.1029/2000RG000095.

Ramachandran, S. and Kedia, S. 2010. Black carbon aerosols over an urban region: Radiative forcing and climate impact. *J. Geophys. Res.* **115**, D10202, doi:10.1029/2009JD013560.

Ramanathan, V., Crutzen, P. J., Kiehl, J. T. and Rosenfeld, D. 2001. Atmosphere—aerosols, climate, and the hydrological cycle. *Science* **294**, 2119–2124.

Ramanathan, V., Chung, C., Kim, D., Bettge, T., Buja, L. and co-authors. 2005. Atmospheric brown clouds: impacts on South Asian climate and hydrological cycle. *Proc. Nat. Acad. Sci. USA* **102**, 5326–5333.

Ramana, M. V., Ramanathan, V., Podgorny, I. A., Pradhan, B. B. and Shrestha, B. 2004. The direct observations of large aerosol radiative forcing in the Himalayan region. *Geophys. Res. Lett.* **31**, L05111, doi:10.1029/2003GL018824.

Remer, L. A., Kleidman, R. G., Levy, R. C., Kaufman, Y. J., Tanré, D. and co-authors. 2008. Global aerosol climatology from the MODIS satellite sensors. *J. Geophys. Res.* **113**, D14S07, doi:10.1029/2007JD009661.

Ricchiazzi, P., Yang, S. R., Gautier, C. and Sowle, D. 1998. SBDART: a research and teaching software tool for plane-parallel radiative transfer in the Earth's atmosphere. *B. Am. Meteorol. Soc.* **79**, 2101–2114.

Sagar, R., Kumar, B., Dumka, U. C., Moorthy, K. K. and Pant, P. 2004. Characteristics of aerosol spectral optical depths over Manora Peak: a high-altitude station in the central Himalayas. *J. Geophys. Res.- Atmos.* **109**, D06207, doi: 10.1029/2003JD003954.

Satheesh, S. K., Moorthy, K. K., Babu, S. S., Vinoj, V. and Dutt, C. B. S. 2008. Climate implications of large warming by elevated aerosol over India. *Geophys. Res. Lett.* **35**, L19809, doi: 10.1029/2008GL034944.

Satheesh, S. K., Moorthy, K. K., Babu, S. S., Vinoj, V., Nair, V. S. and co-authors. 2009. Vertical structure and horizontal gradients of aerosol extinction coefficients over coastal India inferred from airborne lidar

measurements during the Integrated Campaign for Aerosol, Gases and Radiation Budget (ICARB) field campaign. *J. Geophys. Res.- Atm.* **114**, D05204, doi: 10.1029/2008JD011033.

Sikka, D. R. 1997. Desert climate and its dynamics. *Current Science* **72**, 35–46.

Singh, R. P., Dey, S., Tripathi, S. N., Tare, V. and Holben, B. 2004. Variability of aerosol parameters over Kanpur, northern India. *J. Geophys. Res.- Atmos.* **109**, D23206, doi:10.1029/2004JD004966.

Tripathi, S. N., Dey, S., Tare, V., Satheesh, S. K., Lal, S. and co-authors. 2005. Enhanced layer of black carbon in a north Indian industrial city. *Geophys. Res. Lett.* **32**, L12802, doi: 10.1029/2005GL022564.

Tripathi, S. N., Tare, V., Chinnam, N., Srivastava, A. K., Dey, S. and co-authors. 2006. Measurements of atmospheric parameters during Indian Space Research Organization Geosphere Biosphere Programme Land Campaign II at a typical location in the Ganga basin: 1. Physical and optical properties. *J. Geophys. Res.* **111**, D23209, doi: 10.1029/2006JD007278.

Tripathi, S. N., Srivastava, A. B. K., Dey, S., Satheesh, S. K. and Krishnamoorthy, K. 2007. The vertical profile of atmospheric heating rate of black carbon aerosols at Kanpur in northern India. *Atmos. Environ.* **41**, 6909–6915.

Twomey, S. 1974. Pollution and planetary albedo. *Atmos. Environ.* **8**, 1251–1256.

Vadrevu, K. P., Badarinath, K. V. S. and Anuradha, E. 2008. Spatial patterns in vegetation fires in the Indian region. *Environ. Monit. Assess.* **147**, 1–13.

Venkataraman, C., Habib, G., Kadamba, D., Shrivastava, M., Leon, J. F. and co-authors. 2006. Emissions from open biomass burning in India: integrating the inventory approach with high-resolution Moderate Resolution Imaging Spectroradiometer (MODIS) active-fire and land cover data. *Global Biogeochem. Cycles* **20**, GB2013, doi: 10.1029/2005GB002547.

Wang, C., Kim, D., Ekman, A. M. L., Barth, M. C. and Rasch, P. J. 2009. Impact of anthropogenic aerosols on Indian summer monsoon. *Geophys. Res. Lett.* **36**, doi:10.1029/2009GL040114.

Yadav, S. and Rajamani, V. 2004. Geochemistry of aerosols of northwestern part of India adjoining the Thar Desert. *Geochim. Cosmochim. Acta* **68**, 1975–1988.

Winker, D. M., Hunt, W. H. and Hostetler, C. A. 2004. Status and performance of the CALIOP lidar. *Proc. SPIE* **5575**, 8–15.

Yadav, S. and Rajamani, V. 2004. Geochemistry of aerosols of northwestern part of India adjoining the Thar desert. *Geochim. Cosmochim. Acta* **68**, 1975–1988.

Zhu, L., Martins, J. V. and Remer, L. A. 2011. Biomass burning aerosol absorption measurements with MODIS using the critical reflectance method. *J. Geophys. Res.* **116**, D07202, doi:10.1029/2010JD015187.

Supporting Information

Additional Supporting Information may be found in the online version of this article:

Appendix S1. Aerosol characteristics during pre-monsoon
Appendix S2. Aerosol characteristics during monsoon
Fig. S1. (a, b) The 532 nm attenuated backscatter and depolarization profiles from CALIPSO over Kanpur on 31 May at the time of experiment.
Fig. S2. (a) *b*ext and (b) *SSA* from Kanpur to Jaipur on 9 September. *x* and *y* axes represent the latitude and longitude and *z*-axis has the height.
Fig. S3. (a) *b*ext and (b) *SSA* from Kanpur to Bhubaneswar on 12 September, (c) *b*ext and (d) *SSA* from Kanpur to Indore on 14 September and (e) *b*ext and (f) *SSA* from Nagpur to Bhubaneswar on 14 September.

Please note: Wiley-Blackwell is not responsible for the content or functionality of any supporting materials supplied by the authors. Any queries (other than missing material) should be directed to the corresponding author for the article.